THE ASTROPHYSICAL JOURNAL, 453:424–432, 1995 November 1

X-RAY DETECTION OF PSR B1259−63 AT PERIASTRON

V. M. KASPI[1]
IPAC/Caltech/Jet Propulsion Laboratory, Pasadena, CA 91125
M. TAVANI[2]
Columbia Astrophysics Laboratory, New York, NY 10027
F. NAGASE,[3] M. HIRAYAMA,[4] M. HOSHINO,[5] AND T. AOKI[6]
Institute of Space and Astronautical Science, Sagamihara, Kanagawa 229, Japan
N. KAWAI[7]
Institute of Physical and Chemical Research, Wako, Saitama, 351-01, Japan
AND
J. ARONS[8]
Department of Astronomy and Department of Physics, University of California, Berkeley, Berkeley, CA 94720
Received 1995 March 3; accepted 1995 May 11

ABSTRACT

We report on results of X-ray observations of the unique radio pulsar/Be star binary PSR B1259−63, obtained using the *ASCA* satellite 2 weeks before, during, and 2 weeks after the pulsar's most recent periastron passage on 1994 January 9. The source was detected at all three epochs, with an X-ray luminosity in the 1–10 keV band of $\sim 1 \times 10^{34}(d/2\ \mathrm{kpc})^2$ ergs s^{-1} at the pre- and postperiastron epochs, and a factor of ~ 2 smaller at periastron. The X-ray emission can be characterized by power-law spectra with a photon index in the range 1.5–1.9, with evidence for spectral softening at periastron. The photoelectric absorption, $N_{\mathrm{H}} \sim 5 \times 10^{21}$ cm^{-2}, was constant for the three observations within measurement uncertainties and is consistent with the Galactic contribution. We detect no pulsations and derive an upper limit on periodicities close to the PSR B1259−63 spin period of $\sim 7\%$ of the total observed flux, conservatively assuming a sine wave profile. We argue that accretion of gaseous material onto the surface of the neutron star is an unlikely origin for the observed X-rays. The characteristics of the X-ray emission from the PSR B1259−63 system are in good qualitative agreement with models of nonthermal acceleration of relativistic particles from the pulsar wind in a shock at the location at which the pulsar and Be star wind pressures balance. Assuming reasonable Be star equatorial outflow and pulsar wind pressures, we find that the mass-loss rate $\dot{M}$ and surface velocity v are constrained by the relation $100 \lesssim (v/10\ \mathrm{km\ s^{-1}})(\dot{M}/10^{-8}\ M_\odot\ \mathrm{yr}^{-1}) \lesssim 10^4$.

Subject headings: binaries: eclipsing — pulsars: individual (PSR B1259−63) — stars: emission-line, Be — stars: neutron — X-rays: stars

1. INTRODUCTION

PSR B1259−63 is a 47 ms radio pulsar discovered by Johnston et al. (1992b) in a survey of the southern Galactic plane for radio pulsars (Johnston et al. 1992a). Radio timing observations have shown that the pulsar is in a 3.4 yr, highly eccentric binary orbit. The pulsar's astrometric, spin, and orbital parameters, as determined by radio timing (Johnston et al. 1994), are given in Table 1. The pulsar's mass function implies its orbital companion has a mass greater than 3.2 $M_\odot$ assuming a 1.4 $M_\odot$ neutron star. Optical observations have revealed a 10th mag B2 Ve star, SS 2883, at a position coincident with the pulsar's timing position. Johnston et al. (1992b) conclude SS 2883 is the pulsar's companion, and from the spectral type Johnston et al. (1994) deduce a mass for SS 2883 of $\sim 10\ M_\odot$ and a radius of $\sim 6\ R_\odot$. From the dispersion measure of the pulsar and a model for the Galactic electron distribution (Taylor & Cordes 1993), the estimated distance to the system is $d = 4.6$ kpc with approximate uncertainty $\sim 25\%$. Johnston et al. (1994) argue on the basis of photometric observations that the distance to SS 2883 cannot be greater than 1.5 kpc, in conflict with that deduced from the pulsar dispersion measure. We adopt 2 kpc for this paper. A radio eclipse was observed by Johnston et al. (1992b) during the last periastron passage in 1990; however, detailed monitoring of PSR B1259−63 at that epoch was not carried out because only at that epoch was the duplicity recognized.

Be stars show strong Hα emission lines and excess radio and infrared contiuum radiation, which suggest the presence of a dense, slowly expanding wind (e.g., Slettebak 1988 and references therein), while UV observations of resonance lines of C IV and Si IV suggest the presence of a fast, low-density wind (Snow 1982). These seemingly contradictory observations are reconciled in an empirical "disk" model (e.g., Waters 1986) in which the Hα emission and continuum excesses are produced in a slow, dense equatorial wind, with a fast, tenuous wind existing in the polar region. Typical mass-loss rates in the disk regions of Be stars are in the range $10^{-9}\ M_\odot\ \mathrm{yr}^{-1} \lesssim \dot{M} \lesssim 10^{-6}\ M_\odot\ \mathrm{yr}^{-1}$ (e.g., Waters et al. 1988). No direct estimate of the mass-loss rate of SS 2883 has previously been published.

[1] Hubble Fellow; vicky@ipac.caltech.edu.
[2] tavani@carmen.phys.columbia.edu.
[3] nagase@astro.isas.ac.jp.
[4] JSPS Fellow; hirayama@astro.isas.ac.jp.
[5] hoshino@gtl.isas.ac.jp.
[6] aoki@astro.isas.ac.jp.
[7] nkawai@postman.riken.go.jp.
[8] arons@astroplasma.berkeley.edu.

TABLE 1

ASTROMETRIC, SPIN, AND ORBITAL PARAMETERS FOR PSR B1259−63[a]

Parameter	Value
Astrometric, Spin, and Radio Parameters	
Right ascension α(J2000)	$13^h02^m47^s.68$ (2)
Declination, δ(J2000)	$-63°50'08''.6$ (1)
Dispersion measure	146.75 (8) pc cm^{-3}
Period, P	47.762053919 (4) ms
Spin-down rate, $\dot{P}$	$2.2793\ (4) \times 10^{-15}$
Period epoch	MJD 48053.44
Spin-down age, τ	3×10^5 yr
Magnetic field, B	3×10^{11} G
Spin-down luminosity, $\dot{E}$	8×10^{35} ergs s^{-1}
Orbital Parameters	
Orbital period, P_b	1236.79 (1) day
Projected semimajor axis, $a_p \sin i$	1295.98 (1) lt-sec
Longitude of periastron, ω	138°.6548 (2)
Eccentricity, e	0.869836 (2)
Periastron epoch, T_0	MJD 48124.3581 (2)

[a] From Johnston et al. 1994.

Pulsars lose rotational energy by a relativistic wind of electrons, positrons, and possibly heavy ions, which occasionally is seen to energize surrounding gaseous material, resulting in high-energy emission. A well-known example is the Crab Nebula, in which the efficiency of conversion of spin-down energy ($\dot{E} \propto \dot{P}P^{-3}$) into unpulsed X-rays is observed to be $\sim$10%; such high efficiency is believed to be the result of MHD shock acceleration of relativistic pulsar wind particles where the pulsar wind and ambient medium pressures balance (Rees & Gunn 1974; Kennel & Coroniti 1984; Hoshino et al. 1992). Pulsar bow shock nebulae, in which the wind interacts with the interstellar medium, also provide information on pulsar winds (e.g., Bell, Bailes, & Bessell 1993; Cordes, Romani, & Lundgren 1993), however, are expected to be weak high-energy emitters (Arons & Tavani 1993).

In contrast to the environments of other interacting pulsars, PSR B1259−63 allows the study of time-dependent pulsar/nebula interactions because the radio pulsar interacts with the Be star outflow each periastron passage (Kochaneck 1993; Campana et al. 1994; Tavani 1994). If the pulsar radiation pressure is large enough to withstand the compressing ram pressure due to the Be outflow, an interesting time-variable interaction is expected (Tavani, Arons, & Kaspi 1994, hereafter TAK94). Alternatively, for a large Be star mass outflow, accretion can occur. The 69 ms X-ray pulsar A0538−66 is in an eccentric orbit around a Be star and occasionally accretes with an X-ray luminosity near the Eddington limit, demonstrating the ability of mass outflows from massive star companions to cause accretion onto rapidly rotating neutron stars (Skinner et al. 1982).

About 20 Be/neutron star X-ray–emitting binaries are known in the Galaxy. These have orbital characteristics similar to those of PSR B1259−63: long orbital periods and high eccentricities (van den Heuvel & Rappaport 1987). The Be/X-ray binaries form a subclass of the high-mass X-ray binaries, which show pulsed X-ray emission with periods in the range $0.068\ \mathrm{s} \lesssim P \lesssim 10^3$ s, the signature of accretion onto the surface of a strongly magnetized neutron star (Bradt & McClintock 1983). Radio pulsations have never been detected from any high-mass X-ray binary system. The PSR B1259−63 system is therefore unique among Be/neutron star binaries in that the neutron star is also a radio pulsar. Among over 600 known radio pulsars, the PSR B1259−63 system is the only known Be star/pulsar binary. A similar binary system, PSR J0045−7319 in the Small Magellanic Cloud, consists of a 0.926 s pulsar in orbit with a B star. However, optical observations show no evidence for emission lines or any eclipse or anomalous dispersion of the radio signal near periastron (Kaspi et al. 1994; Bell et al. 1995; Kaspi et al. 1995).

X-ray emission was detected from the PSR B1259−63 system near apastron. The first X-ray detection was by Cominsky, Roberts, & Johnston (1994, hereafter CRJ94) who observed the system just after apastron using *ROSAT* in 1992 September. The observed X-ray luminosity in the *ROSAT* band was $0.8\text{–}35 \times 10^{33}$ ergs s^{-1} for $d = 2$ kpc and depending on the assumed spectral model. A recent analysis of public archive *ROSAT* data taken in 1992 February, just before apastron, reveals significant X-ray emission at a level consistent with the CRJ94 result (Greiner, Tavani, & Belloni 1995, hereafter GTB95). Statistics in both detections are poor, and little spectral information is available. Since radio pulsations were detected at the epochs of all *ROSAT* observations, accretion of material onto the neutron star is an unlikely explanation, since it would have quenched the radio emission.

In this paper, we report on a series of three X-ray observations with the *ASCA* satellite at the system's most recent periastron passage. The X-ray observations are part of a multiwavelength campaign organized to study the emission near periastron, including UV and optical emission (McCollum, Castelaz, & Bruhweiler 1995), hard X-ray and gamma-ray emission (Grove et al. 1995), as well as radio wavelengths (Johnston et al. 1995; Manchester et al. 1995). Preliminary reports indicate that the pulsed radio emission became undetectable in 1993 mid-December and became visible again only at the beginning of 1994 February (S. Johnston and R. N. Manchester, private communication). Thus, the *ASCA* observations reported here were all obtained during the radio eclipse.

2. OBSERVATIONS

In order to monitor possible time variability of the X-ray emission, the *ASCA* X-ray satellite observed the system near periastron, and approximately 2 weeks before and after periastron. The first and third observations had exposure times of $\sim$20,000 s, while the second had $\sim$40,000 s. Table 2 gives a summary of the three *ASCA* observations and of the orbital geometry for an assumed Be star mass and radius $M_c = 10\ M_\odot$ and $R_c = 6\ R_\odot$, respectively, and a neutron star mass $M_p = 1.4\ M_\odot$. In the table, ϕ is the true anomaly (at periastron), and s is the pulsar/Be star separation. In Figure 1 we provide a schematic drawing of the pulsar's orbit around the systemic center of mass, together with the approximate location of the pulsar during the X-ray observations reported by CRJ94, GTB95, and those described here.

TABLE 2

SUMMARY OF THE PSR B1259−63 SYSTEM GEOMETRY NEAR THE *ASCA* OBSERVATIONS

Date	MJD	ϕ	s (10^{12} cm)	s/R_c
1993 Dec 28	49349.0	−75°	16	36
1994 Jan 10	49362.2	7	10	24
1994 Jan 26	49378.5	89	18	44

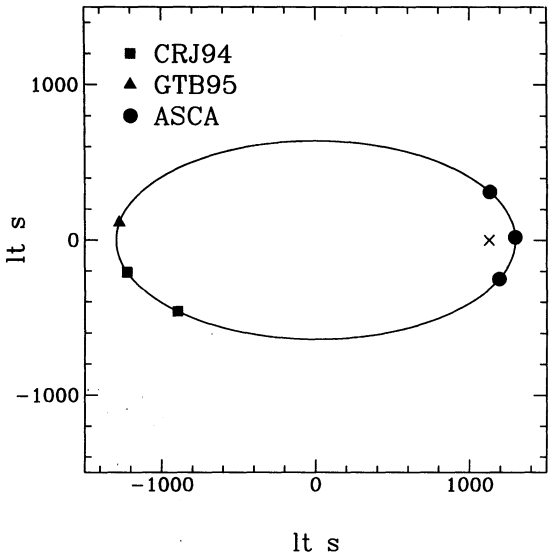

FIG. 1.—Schematic of PSR B1259−63 binary system with the locations of the pulsar during all published X-ray detections indicated. CRJ94 is Cominsky, Roberts, & Johnston (1994); GTB95 is Greiner, Tavani, & Belloni (1995); and the observations labeled ASCA are the subject of this paper. The cross indicates the location of the center of mass of the system.

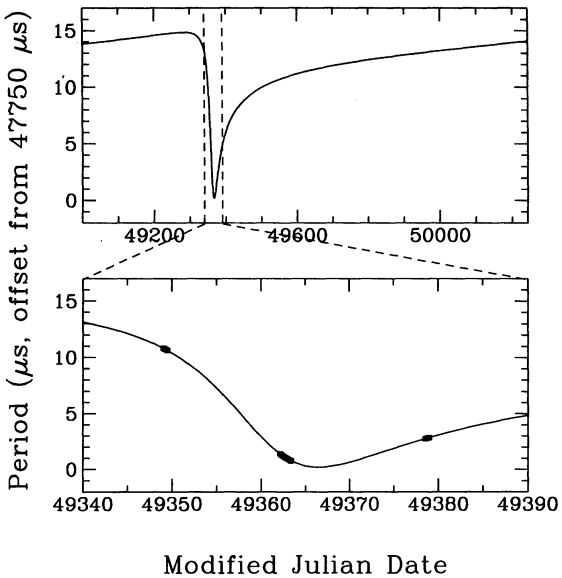

FIG. 2.—PSR B1259−63 velocity curve and the *ASCA* observing epochs. The upper panel is the pulsar's velocity curve as determined from radio timing data (Johnston et al. 1992b). The region between the vertical lines is expanded in the lower panel, in which the epochs of the *ASCA* observations are highlighted.

The *ASCA* satellite (formerly *Astro-D*) carries four X-ray telescopes (XRTs) each consisting of nested concentric thin foils that approximate paired hyperbolic and parabolic surfaces. The X-ray telescopes have bassband 0.5–12 keV and spatial resolution $\sim 1'$. At the focus of two of the telescopes are Solid-state Imaging Spectrometers (SIS), each of which is based around four CCD chips having energy resolution 2% at 5.9 keV and field of view $11' \times 11'$. At the focus of the other two telescopes are Gas Imaging Spectrometers (GIS), imaging gas scintillation proportional counters with 8% energy resolution at 5.9 keV and a circular field of view with diameter $50'$. All of our observations were done using the GIS and SIS in 1-CCD mode. The instruments are described in more detail by Tanaka, Inoue, & Holt (1994) and Serlemitsos et al. (1995).

The data reduction was done at the *ASCA* Guest Observer Facility (GOF) at the Goddard Space Flight Center and at the Institute for Space and Astronautical Science in Japan. The FTOOLS software package was used to identify the pulsar and select a circular region centered on the source from the fields of view of each instrument. For GIS observations, the circular region had radius $6'$, while for the SIS data, the region had radius $4'$. Background subtraction was done using GOF-supplied background files. Hot and flickering pixels were removed from the SIS data. Binned photon lists were created for spectral analyses (rebinning to 64 spectral bins for GIS and 256 for SIS was done after extraction), as were time-tagged photon event files for the timing analyses, with barycentric corrections done using the GOF-supplied software BARYCEN. The pulsar's pulse period as a function of time is plotted in the top panel of Figure 2. The highlighted regions show the epochs and durations of our *ASCA* observations; both the change in observed period from epoch to epoch as well as the small period variation within each observation is apparent. This is discussed further in § 3.2.

Response matrices were produced using GOF-supplied detector response functions and XRT effective area curves using the GOF-supplied ASCAARF software. The GIS data have time resolution 0.976 or 0.488 ms, depending on the telemetry mode, and were used for the timing analysis described below. The SIS data have poor temporal resolution but excellent spectral resolution so were used only for the spectral analysis.

3. RESULTS

At all three observing epochs, a point source was detected at a position consistent with that of the pulsar, given the $\sim 1'$ uncertainty of the *ASCA* pointing. An image from the GIS detector for the second observation is shown in Figure 3;

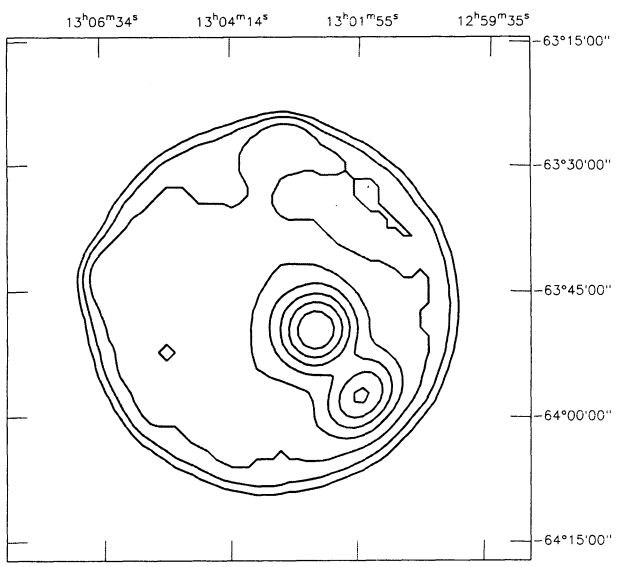

FIG. 3.—Contour plot of the GIS field of view for the MJD 49362 observation. Those for the first two observations are similar. North is up, and west is to the right. Smoothing using a 1 σ width of 1.5 has been applied, and a logarithmic scale used. A total of 12 contour values were used, with contour 5, corresponding to 8 counts per pixel, the first one shown. Contour 12 corresponds to 359 counts per pixel. The brighter source is PSR B1259−63, while the weaker source is an unidentified source unassociated with the PSR B1259−63 system.

TABLE 3

EXPOSURE TIMES AND COUNT RATES[a] FOR THE FOUR *ASCA* INSTRUMENTS FOR EACH OBSERVING EPOCH

	GIS2		GIS3		SIS0		SIS1	
MJD[b]	Exposure (ks)	Count Rate (counts s^{-1})	Exposure (ks)	Count Rate (counts s^{-1})	Exposure (ks)	Count Rate (counts s^{-1})	Exposure (ks)	Count Rate (counts s^{-1})
49349.0.....	27	0.415 (5)	27	0.480 (4)	26	0.626 (5)	26	0.496 (4)
49362.2.....	42	0.217 (2)	42	0.244 (3)	41	0.325 (3)	41	0.263 (3)
49378.5.....	22	0.372 (4)	22	0.429 (5)	19	0.557 (5)	19	0.449 (5)

[a] Background-subtracted count rates not corrected for aspect. The uncertainties shown in parenthesis are 1 σ Poisson uncertainties and do not include systematic uncertainties.

[b] At start of observation.

images of the field for the first and third observations are similar. The brighter source seen in the image is the pulsar. Background-subtracted count rates and exposure times for the four instruments are given in Table 3. Figure 4 shows the light curves for GIS2 data at all three observing epochs; those for the other instruments are similar.

The second source seen in the GIS field of view approximately 10′ southwest of the pulsar system is an unidentified X-ray source. The source was present in all observations but does not appear in the SIS images since it lies outside the smaller field of view. A preliminary analysis suggests the absorption toward this source is $\gtrsim 10^{22}$ cm^{-2}, implying it is more distant than PSR B1259−63. A search through the SIMBAD database reveals no cataloged sources within ∼7′ of this source. We do not consider the serendipitous source further in this paper; however, a more careful analysis is planned.

3.1. *Spectral Results*

The spectral analysis was done with the NASA/GSFC XSPEC software package. Combined SIS0 + SIS1 spectra for the three observations are shown in Figure 5. A simple power law describes the data well at all three epochs, with no evidence for line features. In Table 4 we present results of three-parameter fits to the 256 spectral bin SIS data (SIS0 and SIS1 combined). Although the formal statistical χ^2 values in the table are significantly larger than 1.0, given the systematic uncertainties in the *ASCA* calibration, we consider these fits acceptable. In all cases, the reduced χ^2 is higher for the thermal bremsstrahlung model than for the power-law model. We note that hard X-ray emission in the energy range 50–200 keV from the direction of PSR B1259−63 was detected by the OSSE instrument aboard the *Compton Gamma-Ray Observatory* during an observation in the period 1994 January 3–23 and had a spectrum consistent with a simple extrapolation of the power-law fit to the *ASCA* data reported here (Grove et al. 1995). Also in Table 4 are given 90% confidence upper limits to 6.4 or 6.7 keV emission lines for the power-law model. These were derived assuming a line width of 10 eV. The GIS data are in agreement with the SIS data to within ∼30%, consistent

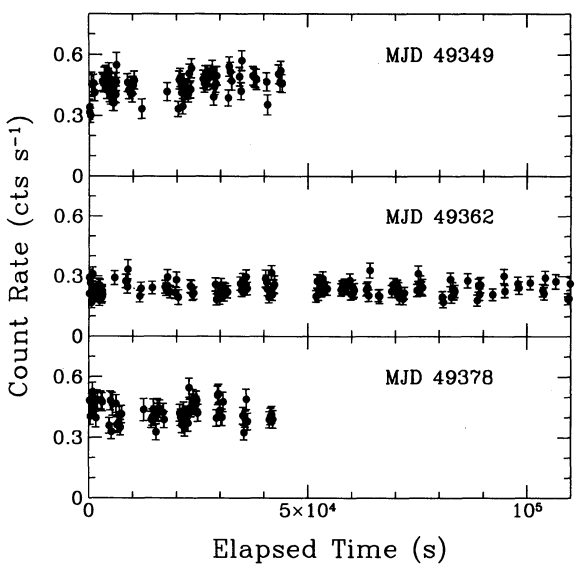

FIG. 4.—GIS2 light curves for PSR B1259−63 at the three observing epochs. The data shown here have been binned in 240 s intervals. Light curves for the other instruments are similar. The GIS2 background count rate is under 10% of the source count rate for all observations.

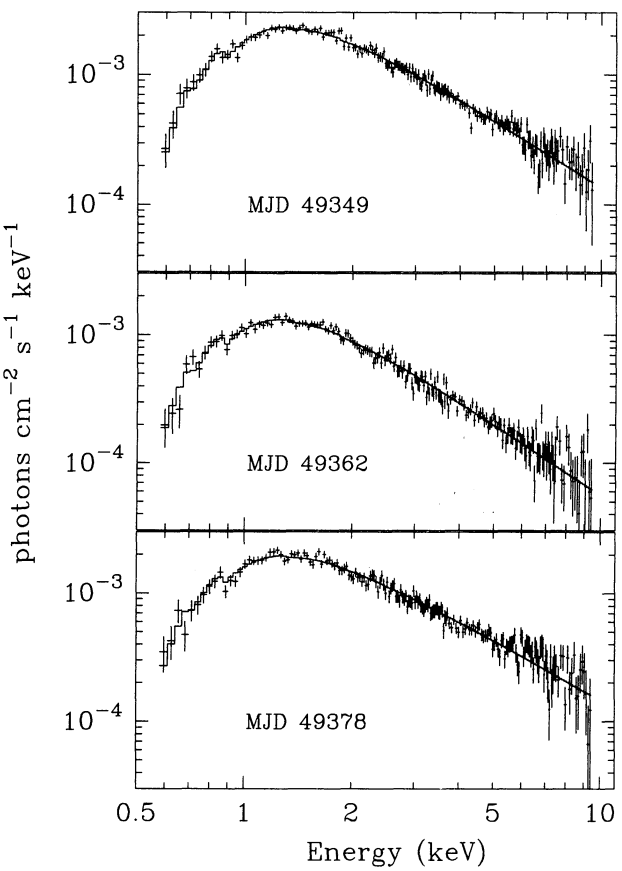

FIG. 5.—*ASCA* SIS spectra at the three observing epochs

TABLE 4

MODEL PARAMETERS[a] FOR *ASCA* SIS OBSERVATIONS OF PSR B1259−63

A. Power Law Model

MJD	N_H (10^{22} cm^{-2})	Photon Index	1–10 keV Flux (10^{-11} ergs cm^{-2} s^{-1})	χ^2_ν	Fe Emission-Line Flux (10^{-6} photons cm^{-2} s^{-1})
49349.0.....	0.56 (2)	1.71 (4)	3.17 (14)	1.08	<7.5
49362.2.....	0.53 (3)	1.86 (4)	1.50 (7)	1.25	<9.8
49378.5.....	0.50 (3)	1.56 (4)	3.04 (16)	1.07	<9.7

B. Thermal Bremsstrahlung Model

MJD	N_H (10^{22} cm^{-2})	kT (keV)	1–10 keV Flux (10^{-11} ergs cm^{-2} s^{-1})	χ^2_ν
49349.0.....	0.45 (2)	9.4 (8)	3.0 (2)	1.28
49362.2.....	0.41 (2)	6.8 (5)	1.42 (8)	1.57
49378.5.....	0.42 (2)	15 (3)	3.0 (3)	1.21

[a] Numbers in parentheses represent 90% statistical uncertainties in the last digit quoted.

with known systematic differences due to calibration uncertainties,[9] and corroborate all SIS spectral trends.

In Figure 6 we show contour plots of the N_H and photon index parameter uncertainties, holding the 1–10 keV flux fixed at the values in Table 4. The contours plotted are 68%, 95%, and 99% confidence levels. There is good evidence for a variation in the photon index, with the steepest index at periastron; however, we find no evidence for any significant variation in the absorption with orbital phase within the measurement uncertainties. The photoelectric absorption toward the source, $N_H = (5.3 \pm 0.5) \times 10^{22}$ cm^{-2}, is consistent with an intrinsically unabsorbed source in the Galactic plane at the estimated distance of PSR B1259−63. Our measurement of N_H is consistent with the approximate values obtained independently near apastron from *ROSAT* observations (CRJ94; GTB95). The observed reddening toward SS 2883, $A_v = 3.25$ mag (Westerlund & Garnier 1989), suggests an approximate expected $N_H \sim 7 \times 10^{21}$ cm^{-2} (Gorenstein 1975), in rough agreement with the value reported here. Finally, as is clear from Table 4, the X-ray flux from the source was time variable, having reached a minimum at periastron that corresponds to about half the values symmetrically around periastron.

3.2. *Search for Pulsations*

X-ray emission modulated with the PSR B1259−63 spin period can be produced by accretion of gaseous material channeled by the relatively strong magnetic field ($B \sim 3 \times 10^{11}$ G) into an X-ray–radiating accretion column. To determine whether accretion is the origin of the observed X-ray emission, we searched for pulsations in the PSR B1259−63 data, using the ephemeris shown in Table 1 provided by the radio data (Johnston et al. 1994). For the timing analysis, only GIS data were used because of their high time resolution. Table 5 summarizes the characteristics of the *ASCA* data that are relevant to the pulsation search. In the table, the MJD is at the start of the observation, T is the duration of the observation (longer than the exposure time because of Earth occultations, South Atlantic Anomaly passages, etc.), N_γ is the total number of GIS photons,[10] P_{app} is the apparent barycentric period at the start of the integration, $\dot{P}_{app}$ is the apparent period derivative due to the pulsar's acceleration in its orbit, and P is the period as observed in a reference frame at rest with respect to the pulsar.

As shown in Figure 2, the pulse period of PSR B1259−63 changed significantly during each of our observations because of the varying Doppler shift due to the large acceleration of the pulsar in its eccentric orbit near periastron. However, the variation in the observed period because of the acceleration of the pulsar is well approximated by a linear trend for our observations. In searching for pulsations, we folded the photons modulo trial periods near the expected pulse period, after having corrected the arrival times for the acceleration of the pulsar in two different ways.

3.2.1. *Epoch-folding with Orbital Doppler Shift Correction*

Prior to searching for pulsations, the orbital Doppler shift of the pulse period was accounted for using standard methods (e.g., Blandford & Teukolsky 1976) and the orbital parameters given by Johnston et al. (1994). Epoch-folding of the corrected photon arrival times was done using the X-ray timing NASA/GSFC software package XRONOS. For each *ASCA* observation, the photons were folded with $j = 32$ time bins across the pulse profile at periods in the interval $P \pm \Delta P$, with $P = 47.7623$ ms. A total of 128 trial periods were searched, with period steps of half the Fourier step, $\delta P = P^2/2T$. The

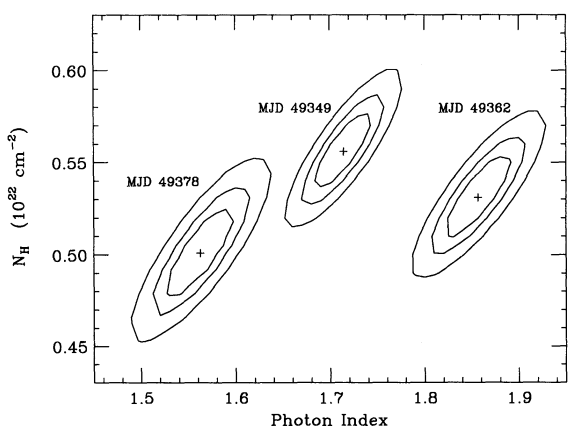

FIG. 6.—Contour plots of the confidence levels for the fit values of N_H and photon index at the three observing epochs. The contours are the 68%, 95%, and 99% confidence levels and were obtained while holding the 1–10 keV flux at the values given in Table 4.

[9] This was compounded in our GIS data because we used a high time resolution mode which required loss of spectral information.

[10] More conservative selection criteria were used in obtaining event lists for the pulsation search. Therefore, the numbers of photons used in the pulsation searches are smaller than would be implied by the count rates reported in Table 3.

TABLE 5

SUMMARY OF CHARACTERISTICS OF THE *ASCA* DATA RELEVANT TO THE PULSATION SEARCH

MJD	T (s)	N_γ	P_{obs} (ms)	$\dot{P}_{obs}$	P (ms)
49349.0.....	44,289	19,899	47.7608264	-4.899×10^{-12}	47.762309
49362.2.....	110,447	18,496	47.7514099	-5.739×10^{-12}	47.762311
49378.5.....	46,113	15,787	47.7527459	$+2.647 \times 10^{-12}$	47.762314

period range ΔP was 1.5 μs for the first and third observations and 0.6 μs for the second observation.

For each trial period, the quantity

$$S = \sum_{k=1}^{j} \frac{(C_k - C)^2}{\sigma_k^2}, \quad (1)$$

where C_k is the observed count rate of the kth phase bin, C is the average count rate, and $\sigma_k^2 = jC/T$ (Leahy et al. 1983) was computed. A coherent pulsation in the data results in a value for S large compared with noise. No statistically significant peak in the S versus trial period distributions for any of the three observations was detected. Using the analytical methods described by Leahy et al. (1983), we have computed 90% confidence upper limits on the pulsed fractions, conservatively assuming a sine wave profile. These are given in column (2) of Table 6.

Similar epoch-folding analyses were done on short stretches of data in which the variable Doppler shift was negligible. Also, searches were done on the GIS2 and GIS3 data sets separately, in case an unknown clock discrepancy exists between the two instruments. In addition, a similar analysis was done using epoch-folding and the Z_n^2 test (Buccheri et al. 1983) for $n = 2, 3$. In no instance was there any evidence for pulsations in the data.

We also peformed an epoch-folding search on two subsets of the data in energy bands 0.5–2 keV and 2–10 keV. The photon arrival times corrected for the orbital motion were folded at trial periods in the range $P \pm \Delta P$, where $P = 47.7623$ ms and $P = 1$ μs. The Fourier step was used for the period increment. The number of phase bins across a trial profile was $j = 32$. The estimator S was calculated for each trial period, and inspection of distributions of S versus P revealed no significant features. Upper limits to the pulsed fractions obtained in each spectral band for combined GIS2 + GIS3 were calculated using the techniques described by Leahy et al. (1983) and are provided in columns (3) and (4) of Table 6. Furthermore, epoch-folding searches in the same two spectral bands were done using the Z_n^2 test for $n = 1, 2, 3, 4$. Finally, the GIS2 and GIS3 data sets were searched separately in an analogous way. No evidence for pulsations was found.

TABLE 6

90% CONFIDENCE UPPER LIMITS ON PULSATIONS FROM EPOCH-FOLDING SEARCHES DONE WITH AN ORBITAL DOPPLER SHIFT CORRECTION

MJD (1)	0.5–10 keV GIS2 + GIS3 (2)	0.5–2 keV GIS2 + GIS3 (3)	2–10 keV GIS2 + GIS3 (4)
49349.0.....	0.066	0.100	0.077
49362.2.....	0.069	0.109	0.093
49378.5.....	0.075	0.119	0.090

3.2.2. *Epoch-folding by Searching in P-$\dot{P}$ Space*

Since the variation in the pulse period due to the orbit over the course of each observation is well approximated by a linear trend, as an additional check, we searched for pulsations in P-$\dot{P}$ space. This "acceleration search" is motivated by the possibility of small biasing of the orbital parameters obtained by Johnston et al. (1994) using radio timing, due perhaps to unmodeled dispersion delays, unmodeled post-Keplerian dynamical effects (Kochaneck 1993; Lai, Bildsten, & Kaspi 1995), or because their determination was based on fewer than two orbits. Since XRONOS cannot do acceleration searches, it was not used for this part of the analysis.

With no variable Doppler shift correction done to the photon arrival times, they were folded at a range of trial P's and $\dot{P}$'s using 8, 16, and 32 bins across the pulse period, to ensure sensitivity to a variety of pulse duty cycles. Steps in P were done oversampling the Fourier step by a factor of 5. The optimal step in $\dot{P}$ was chosen to be that which results in the worst case photon arrival time 180° out of phase with the pulse, $\delta\dot{P} = (P/T)^2$, also oversampled by a factor of 5. Parameters for this search are given in Table 7. The statistic S was computed for each folded profile. Plots of S versus P and $\dot{P}$ were examined for significant features; none was found. To estimate an upper limit to the pulsed fraction, fake pulsed photon arrival times were injected into the data. The fraction of fake arrival times was adjusted until it produced a feature in the S distribution consistent with features seen in the real data. Using this method, we conclude that for pulse profiles having widths less than one-eighth of the pulse period, less than 2% of the flux was pulsed at each epoch.

4. DISCUSSION

We consider here various origins of the X-ray emission from the PSR B1259−63 system near periastron.

4.1. *X-Ray Emission from the Be Star*

Early-type B stars have been shown to emit X-rays that are explained as originating from a line-driven wind heated by shocks (Lucy 1982; MacFarlane & Cassinelli 1989; Bjorkman & Cassinelli 1993), with X-ray luminosity, L_x, observed to scale roughly with bolometric luminosity, L_{bol}, with proportionality constant $\sim 10^{-7}$ (Pallavicini et al. 1981). In a recent *ROSAT*

TABLE 7

SUMMARY OF P-$\dot{P}$ PULSATION SEARCH

MJD	P Range (ms)	$\dot{P}$ Range ($\times 10^{-12}$)
49349.0.....	47.7600–47.7616	−20.0 to 0.0
49362.2.....	47.7510–47.7520	−7.0 to −4.0
49378.5.....	47.7520–47.7535	0.0 to 18.0

survey of OB and OBe stars by Meurs et al. (1992), a similar relationship was found, albeit with considerable scatter, with *ROSAT* L_x/L_{bol} ranging from 10^{-8} to 10^{-4}, and no significant difference between X-ray luminosities of OB stars and OBe stars. Using our observed *ASCA* X-ray fluxes extrapolated to the *ROSAT* band and the bolometric luminosity for SS 2883 reported by Johnston et al. (1992b) of $5.8 \times 10^4\ L_\odot$, we have $L_x/L_{bol} = 5 \times 10^{-5}$ for the pre- and post-periastron observations, and half that at periastron. Although this is much larger than would be predicted by the above relationship, it is consistent with the observed scatter. However, Cassinelli et al. (1994) showed that X-ray spectra of main- and near–main-sequence B stars are characterized by emission from gas at a temperature of $\sim 2 \times 10^6$ K, with the brightest X-ray source in their sample having temperature 9.3×10^6 K. By contrast, our thermal spectrum fits to the *ASCA* data for PSR B1259−63 are characterized by much higher temperatures, $T \sim 10^8$ K (see § 3.1). In any case, as discussed in § 3.1, OSSE observations by Grove et al. (1995) rule out a thermal spectrum. Finally, the increase in X-ray luminosity from apastron to periastron is most reasonably attributed to the location of the pulsar with respect to the Be star. We conclude that the Be star is an unlikely source of the observed X-rays reported here.

We note that the X-ray luminosities reported by both CRJ94 and GTB95 also imply L_x/L_{bol} that, though large compared to the $L_x/L_{bol} \simeq 10^{-7}$ rule of thumb, are within the scatter in the observations reported by Meurs et al. (1992) (see also Campana et al. 1994). Since CRJ94 and GTB95 had insufficient statistics for precise determination of spectral parameters, a thermal model with temperatures consistent with those reported for OB stars by Cassinelli et al. (1994) could not be excluded. Thus, although coronal emission as the origin of the apastron X-rays is unlikely, it cannot be ruled out with certainty without more sensitive observations.

4.2. *X-Ray Emission from the Neutron Star Surface or Magnetosphere*

Short-period pulsars are occasionally observed to emit X-rays (see Ögelman 1995 for a review). Although high-energy emission is generally associated with pulsars having much smaller characteristic ages than that of PSR B1259−63, its short pulsation period of 47 ms makes it a plausible X-ray emitter. X-rays from isolated neutron stars are observed in two different forms: X-rays are produced either in the form of pulsations (e.g., Seward & Harnden 1982; Seward, Harnden, & Helfand 1984) or in weak unpulsed thermal emission arising from the cooling of the neutron star (e.g., Córdova et al. 1989 Halpern & Ruderman 1993). The unpulsed and hard nonthermal emission rules out both these possibilities.

4.3. *X-Ray Emission from Accretion onto the Neutron Star Surface*

The gravitational accretion radius is given by

$$R_G \equiv \frac{2GM_p}{v_{rel}^2} \simeq \frac{3 \times 10^{12}\ \mathrm{cm}}{(v_{rel}/100\ \mathrm{km\ s^{-1}})^2}, \quad (2)$$

where v_{rel} is the relative wind/orbital velocity. For reasonable assumptions about the pressures of the pulsar and Be star winds, the radius at which the two pressures balance is likely to be well outside the accretion radius, at all orbital phases (Kochaneck 1993; Campana et al. 1994; TAK94). Accretion is thus unlikely to occur, even near periastron, unless the Be star possesses an unusually strong wind. For a discussion of accretion in the context of the apastron X-ray detections, see CRJ94 and GTB95.

Parameterizing the Be star wind by $\Upsilon \equiv \dot{M}_{-8} v_6$, where the Be star mass-loss rate $\dot{M} \equiv (10^{-8}\ M_\odot\ \mathrm{yr}^{-1})\dot{M}_{-8}$ and the surface wind velocity $v \equiv (10^6\ \mathrm{cm^{-1}\ s^{-1}})v_6$, TAK94 showed that accretion was possible near periastron only for $\Upsilon \gtrsim 10^4$ for standard pulsar wind parameters and characteristics of the Be star outflow. However, under these conditions, accretion onto the neutron star should yield an X-ray luminosity several orders of magnitude larger than is observed.

Other evidence against the accretion scenario is provided by the absence of X-ray pulsations at any orbital phase. The surface magnetic field strength of PSR B1259−63 is $B = 3.3 \times 10^{11}$ G, which should be more than sufficient to channel any infalling matter onto the stellar surface near the poles, which should result in a strongly anisotropic angular pattern of emission (Nagase 1989). The observability of X-ray pulsations from the PSR B1259−63 system depends somewhat on the geometry of inclination of the pulsar magnetic axis with respect to the line of sight; however, accretion without pulsations requires finely tuned geometries.

There are additional arguments against accretion. Spectra at all three epochs show no features, such as iron Kα emission lines, seen in spectra of known accreting, high magnetic field systems (Nagase 1989). Also, the OSSE results demonstrate the absence of any spectral cutoff, commonly observed in accreting systems (White, Swank, & Holt 1983). Furthermore, a fourth *ASCA* observation of PSR B1259−63 made after the radio pulsations reappeared (Hirayama et al. 1995) shows very similar X-ray characteristics to those reported here, rendering an accretion scenario, in which radio pulsations should be quenched, highly unlikely. In addition, the stability of the X-ray emission during each observation (Fig. 4), the absorption being consistent with the Galactic contribution, and the observed lack of variation of N_H with orbital phase, though not strong arguments against accretion, certainly provide no evidence for it.

Finally, we note that Manchester et al. (1995) report very small perturbations in the pulsar's rotation period ($\Delta P/P \approx 10^{-9}$) using radio timing observations pre-and postperiastron, which they interpret as being due to torques induced from the interaction of the pulsar and Be star wind in a propeller regime. This interpretation predicts a periastron X-ray luminosity much smaller than we have observed. Although our results cannot rule out brief, strong Be star outbursts between *ASCA* observations, more likely interpretations of the timing results are biasing of the orbital parameters by unmodeled dispersion or scattering, or by dynamical effects (Kochaneck 1993; Lai et al. 1995). In any case, that Manchester et al. (1995) observed such small timing perturbations provides additional evidence against an accretion origin for the X-rays reported here.

4.4. *X-Ray Emission from Captured Material Outside the Pulsar Light-Cylinder*

King & Cominsky (1994) proposed a model to explain the observed apastron X-rays as being due to the release of gravitational potential energy of gaseous material falling as far as a boundary radius, defined to be the location at which the pulsar magnetic pressure balances the ram pressure of the infalling gas. In this model, the boundary radius, unlike the canonical magnetospheric radius, is located outside of the light cylinder. The motivation for such a scenario came from the fact that at

apastron, both radio pulsations and X-ray emission were detected. At apastron, King & Cominsky (1994) found a boundary radius very close (within a factor of 2) to the light cylinder;[11] at periastron where the Be star wind density is at least three orders of magnitude larger, it is difficult to see how matter, if it could overcome the pulsar wind pressure, would not penetrate the light cylinder and result in standard accretion, already discussed in § 4.3 above. Thus, this model does not appear applicable to the periastron region.

4.5. *Shock Emission*

The difficulties encountered by canonical accretion and gravitational capture models in explaining the characteristics of the X-ray emission from the PSR B1259−63 system suggest an alternative mechanism is at work. A natural candidate for the origin of the unpulsed X-rays of moderate luminosity and low photoelectric absorption reported in this paper is magnetohydrodynamic shock-powered radiation. Shock acceleration of the Crab pulsar pairs accounts well for many of the spectral and morphological properties of the high-energy emission from the Crab Nebula (Kennel & Coroniti 1984; Gallant & Arons 1994). The contact discontinuity region at the boundary between the decelerated pulsar wind and the Be star wind is the likely site of analogous shock particle acceleration in the PSR B1259−63 system (TAK94). A shocked Be star wind cannot account for the large X-ray luminosities that we have observed (Kochaneck 1993).

As discussed by TAK94, there are two important radiative cooling mechanisms that can be effective in the PSR B1259−63 system. One is synchrotron cooling of the pairs in the pulsar magnetic field, which becomes more efficient as the shock approaches the pulsar. The other is inverse-Compton scattering in the optical photons from the radiating photosphere of the Be star, which becomes more efficient as the shock approaches the Be star. However, if the shock acceleration time is short compared to radiative cooling timescales, the flow in and just behind the shock is nonradiative, and shock acceleration is able to achieve a pair power-law spectrum. For a range of wind parameters in the PSR B1259−63 system corresponding to a shock located at intermediate distances between the pulsar and Be star, TAK94 showed that the shock acceleration timescale is shorter than the cooling timescales. In this regime, a nonthermal spectrum is expected and will extend from X-ray energies to ∼1–10 MeV for a relativistic Lorentz factor of electron/positron pairs, $\gamma \sim 10^6$, similar to that found in models of the response of the Crab Nebula to the wind from its pulsar.

The nonthermal nature of the *ASCA* spectrum from the PSR B1259−63 system, as corroborated by the OSSE detection (Grove et al. 1995), does not agree with the quasithermal spectrum expected in the case of $\Upsilon \lesssim 100$ by strong inverse-Compton cooling for a shock radius close to the surface of the Be star. Our results favor a shock radius at an intermediate distance between the Be star and PSR B1259−63, with $\Upsilon \gtrsim 100$, and a shock acceleration timescale less than or comparable with the synchrotron timescale near periastron (case A of the nonthermal "compact" nebular emission of TAK94). The observed efficiency of conversion of spin-down pulsar energy into X-ray emission in the *ASCA* band at periastron is $L_x/\dot{E} \simeq 0.9(d/2\ \mathrm{kpc})\%$ and approximately twice this value at the pre- and postperiastron epochs. The variability of the X-ray emission and spectrum of the PSR B1259−63 system near periastron can be due to an increase of synchrotron cooling near periastron with consequent modification of the emission properties of the shock, including a change in luminosity as well as a change in photon index, as is observed. Alternatively, it could be due to a misalignment between the orbital plane and the Be star disk (Lai et al. 1995). A detailed study of the constraints on the shock acceleration physics and on the complex interplay among radiation mechanisms for the PSR B1259−63 system is beyond the scope of this paper and will be presented elsewhere (Tavani & Arons 1995).

[11] We note that King & Cominsky (1994) used a dipolar magnetic field outside the light cylinder in their pressure balance calculation. Using the correct $1/r$ field dependence does not change this result much for their input parameters.

5. CONCLUSIONS

We have reported on three X-ray observations of the unique radio pulsar/Be star binary system PSR B1259−63 obtained near periastron using the *ASCA* satellite. At all three epochs, the source was observed to have moderate X-ray luminosity $\sim 10^{34}$ ergs s^{-1} in the *ASCA* band and absorption $N_{\mathrm{H}} \sim 5 \times 10^{21}$ cm^{-2}, consistent with that expected from the Galactic contribution alone. No X-ray pulsations were detected. The observed X-ray spectra are all consistent with simple power laws. Some of the X-ray characteristics varied in the three observations: the X-ray luminosity was a factor of ∼2 smaller, and there was some evidence for a softening of the spectrum at periastron. The absorption, by contrast, was constant for the three observations.

We conclude that accretion onto the neutron star is an unlikely explanation for the observed X-rays, both those reported here and those observed near apastron. Any model involving accretion would have to explain the following observations, none of which is typical of other known accreting sources: a radio pulsar wind pressure was overcome with only moderate X-ray luminosity; no pulsations were detected in spite of a high neutron star magnetic field; no features were observed in spectrum; no spectral cutoff was observed; radio pulsations were visible near the same epoch as the X-rays (Hirayama et al. 1995); and no large perturbations from radio pulse timing done before and after periastron were observed (Manchester et al. 1995). The absence of accretion strongly suggests the Be star wind could not overcome the pulsar wind pressure, which implies $\Upsilon \lesssim 10^4$ for reasonable pulsar and Be star wind parameters (TAK94).

By contrast, magnetohydrodynamic shock acceleration of relativistic electron/positron pulsar wind pairs provides a natural way to account for all the observations reported here. In the framework outlined by TAK94, our observations constrain the Be star wind to have $\Upsilon \gtrsim 100$. A detailed interpretation of the results reported here in terms of the shock acceleration mechanism will appear elsewhere (Tavani & Arons 1995).

Careful monitoring of high-energy emission from PSR B1259−63 at other orbital phases will be useful for further constraining properties of the pulsar wind and the shock acceleration mechanism. Be stars are well known to have episodes of enhanced mass loss, and the possibility of accretion of Be star wind material onto the neutron star during a future outburst, especially near periastron, cannot be discounted. However, as discussed by CRJ94, there is no evidence in existing X-ray archives for outbursts for the past seven periastron passages.

We are indebted to the staff of the *ASCA* Guest Observers Facility, especially to K. Ebisawa, E. Gotthelf, N. White, and L. Angeli. This work was supported via NASA grant NAG 5-2730. We thank D. Chakrabarty, L. Cominsky, J. Halpern, T. Hamilton, F. Harrison, S. Johnston, M. van Kerkwijk, and R. N. Manchester for useful discussions. V. M. K. received support through a Princeton University Higgins Instructorship and from NASA via a Hubble Fellowship through grant HF-1061.01-94A from the Space Telescope Science Institute, which is operated by the Association of Universities for Research in Astronomy, Inc., under NASA contract NAS 5-26555. Part of this research was carried out at the Jet Propulsion Laboratory, California Institute of Technology, under contract with the National Aeronautics and Space Administration. M. T. acknowledges support by the GRO Fellowship GRO/PFP-91-23. M. H. is a fellow of the Japan Society for the Promotion of Science. This research has made use of the SIMBAD database, operated at CDS, Strasbourg, France.

REFERENCES

Arons, J., & Tavani, M. 1993, ApJ, 403, 249
Bell, J. F., Bailes, M., & Bessell, M. S. 1993, Nature, 364, 603
Bell, J. F., Bessell, M. S., Stappers, B., Bailes, M., & Kaspi, V. M. 1995, ApJ, 447, L117
Bjorkman, J. E., & Cassinelli, J. P. 1993, ApJ, 409, 429
Blandford, R., & Teukolsky, S. A. 1976, ApJ, 205, 580
Bradt, H. V. D., & McClintock, J. E. 1983, ARA&A, 21, 13
Buccheri, R., et al. 1983, A&A, 128, 245
Campana, S., Stella, L., Mereghetti, S., & Colpi, M. 1994, A&A, in press
Cassinelli, J. P., Cohen, D. H., MacFarlane, J. J., Sanders, W. T., & Welsh, B. Y. 1994, ApJ, 421, 705
Cominsky, L., Roberts, M., & Johnston, S. 1994, ApJ, 427, 928 (CRJ94)
Cordes, J. M., Romani, R. W., & Lindgren, S. C. 1993, Nature, 362, 133
Córdova, F. A., Hjellming, R. M., Mason, K. O., & Middleditch, J. 1989, ApJ, 345, 451
Gallant, Y. A., & Arons, J. 1994, ApJ, 435, 230
Gorenstein, P. 1975, ApJ, 198, 95
Greiner, J., Tavani, M., & Belloni, T. 1995, ApJ, 441, L43 (GTB95)
Grove, E., Tavani, M., Purcell, W. R., Kurfess, J. D., Strickman, M. S., & Arons, J. 1995, ApJ, 447, L13
Halpern, J., & Ruderman, M. 1993, ApJ, 415, 286
Hirayama, M., Nagase, F., Tavani, M., & Kaspi, V. M. 1995, in preparation
Hoshino, M., Arons, J., Gallant, Y. A., & Langdon, A. B. 1992, ApJ, 390, 454
Johnston, S., Lyne, A. G., Manchester, R. N., Kniffen, D. A., D'Amico, N., Lim, J., & Ashworth, M. 1992a, MNRAS, 255, 401
Johnston, S., Manchester, R. N., Lyne, A. G., Bailes, M., Kaspi, V. M., Qiao, G., & D'Amico, N. 1992b, ApJ, 387, L37
Johnston, S., Manchester, R. N., Lyne, A. G., D'Amico, N., Gaensler, B. M., & Nicastro, L. 1995, MNRAS, submitted
Johnston, S., Manchester, R. N., Lyne, A. G., Nicastro, L., & Spyromilio, J. 1994, MNRAS, 268, 430
Kaspi, V. M., Johnston, S., Bell, J. F., Manchester, R. N., Bailes, M., Bessell, M., Lyne, A. G., & D'Amico, N. 1994, ApJ, 423, L43
Kaspi, V. M., Manchester, R. N., Bailes, M., & Bell, J. F. 1995, in IAU Symp. 165, Compact Stars in Binaries, ed. J. van Paradijs, E. P. J. van den Heuvel, & E. Kuulkers (Dordrecht: Kluwer), in press
Kennel, C. F., & Coroniti, F. V. 1984, ApJ, 283, 694
King, A., & Cominsky, L. 1994, ApJ, 435, 411
Kochanek, C. S. 1993, ApJ, 406, 638
Lai, D., Bildsten, L., & Kaspi, V. M. 1995, ApJ, 452, 819
Leahy, D. A., Darbro, W., Elsner, R. F., Weisskopf, M. C., Sutherland, P. G., Kahn, S., & Grindlay, J. E. 1983, ApJ, 266, 160
Lucy, L. B. 1982, ApJ, 255, 286
MacFarlane, J. J., & Cassinelli, J. P. 1989, ApJ, 347, 1090
Manchester, R. N., Johnston, S., Lyne, A. G., D'Amico, N., Bailes, M., & Nicastro, L. 1995, ApJ, 445, L137
McCollum, B., Castelaz, M. W., & Bruhweiler, F. C. 1995, in preparation
Meurs, E., et al. 1992, A&A, 265, L41
Nagase, F. 1989, PASJ, 41, 1
Ögelman, L. 1995, in ASP Conf. Ser. 72, Millisecond Pulsars: A Decade of Surprise, ed. A. Fruchter, M. Tavani, & D. Backer (San Francisco: ASP), 309
Pallavicini, R., Golub, L., Rosner, R., & Vaiana, G. 1981, ApJ, 258, 279
Rees, M. J., & Gunn, J. E. 1974, MNRAS, 167, 1
Serlemitsos, P. J., et al. 1995, PASJ, 47, 105
Seward, F. D., & Harnden, F. R. 1982, ApJ, 256, L45
Seward, F. D., Harnden, F. R., Helfand, R. F., Leahy, D., Weisskopf, M. C., & Grindlay, J. 1982, Nature, 297, 568
Skinner, G. K., Bedford, D. K., Elsner, R. F., Leahy, D., Weisskopf, M. C., & Grindlay, J. 1982, Nature, 297, 568
Slettebak, A. 1988, PASP, 100, 700
Snow, T. P. 1982, ApJ, 253, L39
Tanaka, Y., Inoue, H., & Holt, S. S. 1994, PASJ, 46, L37
Tavani, M. 1994, in The Gamma-Ray Sky with *Compton GRO* and SIGMA, ed. M. Signore, P. Salati, & G. Vedrenne (Dordrecht: Kluwer), in press
Tavani, M., & Arons, J. 1995, in preparation
Tavani, M., Arons, J., & Kaspi, V. M. 1994, ApJ, 433 L37 (TAK94)
Taylore, J. H., & Cordes, J. M. 1993, ApJ, 411, 674
van den Heuvel, E. P. J., & Rappaport, S. 1987, in Physics of Be Stars, ed. A. Slettebak, & T. P. Snow (Cambridge: Cambridge Univ. Press), 291
Waters, L. B. F. M. 1986, A&A, 162, 121
Waters, L. B. F. M., Taylor, A. R., van den Heuvel, E. P. J., Habets, G. M. H. J., & Persi, P. 1988, A&A, 198, 200
Westerlund, B. E., & Garnier, R. 1989, A&AS, 78, 203
White, N. E., Swank, J. H., & Holt, S. S. 1983, ApJ, 270, 711